Radiation Measurements Over a Snowfield at an Elevated Site

By
Hans C. Korff, Jeffrey J. Gailiun and Thomas H. Vonder Haar

Department of Atmospheric Science
Colorado State University
Fort Collins, Colorado

January 1974

Colorado State University

Department of Atmospheric Science

Paper No. 221

RADIATION MEASUREMENTS OVER A SNOWFIELD AT AN ELEVATED SITE

by

Hans C. Korff*
Jeffrey J. Gailiun
Thomas H. Vonder Haar

*Meteorologisches Institut der Universitaet Bonn, D-53 Bonn, Auf dem Huegel 20, West Germany

ABSTRACT

For several days at the end of January and the beginning of February 1972, the components of short-wave radiation were measured over a snowfield in a valley of the Rocky Mountains at a height of 2700 m above sea level. Global and reflected radiation were obtained by a set of Eppley pyranometers. In addition, the direct solar radiation and the turbidity of the atmosphere were derived from pyrheliometric data on cloud-free days.

Main interest was given to the reflectance of the snowfield in relation to the position of the sun, especially at low elevation angles. These reflectance values were measured for cloudless as well as for cloudy days and compared with those published by other authors for arctic and antarctic conditions.

TABLE OF CONTENTS

LIST OF FIGURES

RADIATION MEASUREMENTS OVER A SNOWFIELD AT AN ELEVATED SITE

1.0 INTRODUCTION

The effect of the radiative properties of a snowfield on the heat budget has been studied by several authors in the Arctic and Antarctic (Rusin, 1964). They show that due to the high reflectivity for solar radiation together with an extreme thermal emissivity, the incoming energy hardly balances the outgoing loss, even in summer, when the pole receives more global radiation on a clear day than a point on the equator (Korff, 1971).

With polar orbiting satellites it became possible to observe the radiation budget of the earth-plus-atmosphere system in these remote areas regularly on a large scale basis (Vonder Haar and Suomi, 1971). But for the investigation of the atmospheric energetics this could only be the first step. Next we have to look at the atmosphere and earth budgets separately (Lettau and Lettau, 1969). This requires the knowledge of the reflectivity of the surface as well as the transparency of the atmosphere, at least in a parameterized form. To obtain this information for application to polar studies, measurements of shortwave radiation were made over a snowfield at Pingree Park in the Colorado Rockies.

In addition to the general experiment objectives noted above, the Pingree Park data were used to check a snow reflectance model used in processing radiation budget measurements from the Nimbus-3 satellite.

2.0 THE INSTRUMENTS

2.1 The Pyranometer

To measure the global and reflected radiation, a set of Eppley Black and White Pyranometers was used, with element No. 8-48/11110 facing upward and element No. 8-48/10958 facing downward. To provide a more suitable separation of the radiative energy from the upper and the lower hemispheres two aluminum plates with a diameter of 24 cm were attached to the instrument at the level of the thermopiles. The whole system was ventilated to avoid severe temperature gradients inside the body. To remove snow and ice from the sensors without disturbing the environment, the ventilated air could be heated. During the measurements, however, the heating element was not used.

The instrument was horizontally leveled and placed about 1 m above the snowfield. To provide an undisturbed field of view of at least 55° in radius for the lower sensor, the radiometers were mounted to a 1.5 m long boom. The field of view of the upper sensor was free from any kind of instrumentation and only limited by the natural horizon.

The output of the pyranometers was recorded on a compensating dual channel Honeywell recorder. It was placed inside the laboratory, about 150 m from the site. The connecting electric leads had a total resistance of 4.0Ω. A sample of the record is shown in Fig. 3. It had a resolution in time of 25 cm/hour and an amplitude of 1.5 cm/mV with a total scale width of 15 cm.

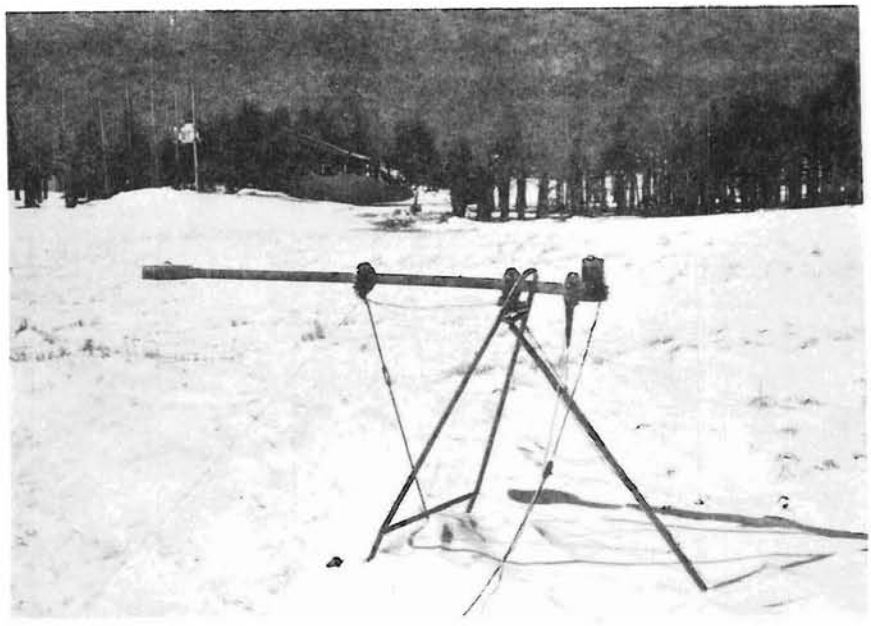

Fig. 1. Pyranometer unit in position

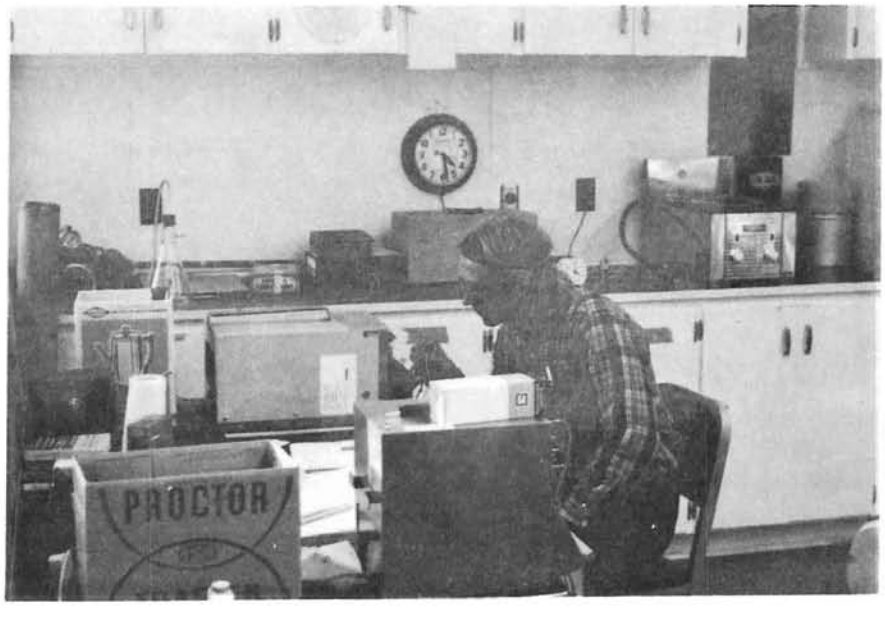

Fig. 2. Recording units in the laboratory

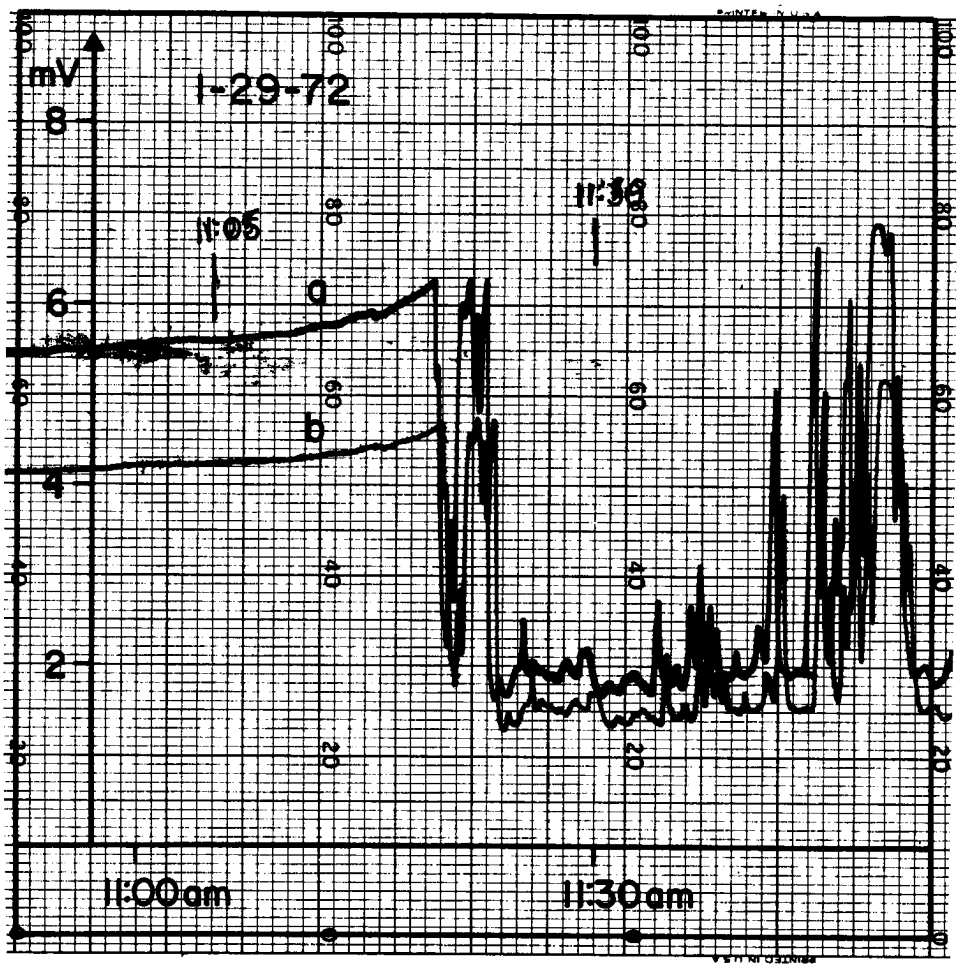

Fig. 3. Sample section of pyranometer chart output
(a) incoming radiation (b) reflected radiation
Cumulus clouds occurred after 11:19 a.m.

2.2 The Pyrheliometer

The direct solar radiation was observed with an Eppley Normal Incidence Pyrheliometer type NIP No. 11095E6. It was equipped with a set of the Schott standard glass filters OG 1, RG 2 and RG 8. For sun tracking, the instrument was attached to an equatorial telescope mount with an electric clock drive.

Fig. 4. Recording pyrheliometric observations

The incoming energy was indicated on a manually compensated Leeds & Northrup galvanometer. Its scale had an accuracy of 1/100 of a mV.

2.3 The Calibration of the Instruments

The pyrheliometer was calibrated by the manufacturer. For the range of accuracy, we accepted the standards recommended by the WMO (1971), thus setting a calibration factor of 5.17 ± 0.03 mV/ly min^{-1}. For our calculations we supposed the window material of the instrument to be transparent for the entire solar spectrum. The short-wave "cut-off" characteristic of the filters was checked for the range

from 0.50 to 0.96 µm with an Hitachi Perkin-Elmer UV = VIS Spectrophotometer. The results calculated gave the following filter-factors:

Filter	OG 1	RG 2	RG 8
Filterfactor	1.1043	1.1033	1.1044
Temperature dependency in µm/°C	.12	.14	.18

(1) Filterfactor:

The measurements were made at a temperature of 25°C. The shift of the "cut-off" to lower wavelength with decreasing temperature was taken into account by the values given by Ångström and Drummond (1959) and shown in the table above.

The calibration of the pyranometers was made on site by the "shading-method" as recommended by CSAGI (1958) and WMO (1971) (see Appendix I). For this the pyrheliometer served as the standard instrument. From several measurements we calculated a sensitivity of 6.81 ± 0.06 mV/ly min^{-1} for element No. 11110 and 6.60 ± 0.06 mV/ly min^{-n} for element No. 10958 for sun positions between 57° and 60° zenith distance.

Special attention was given to the fact that the radiation from below is more or less isotropic while the radiation from above is mainly direct, for clear sky conditions (Stanhill, Fuchs, Oguntoyinbo, 1971). As shown by Dirmhirn (1959) the observed sensitivity of most pyranometers corresponds very well to that calculated from normal incidence energy and the cosine of the incidence angle down to 70° zenith distance.

A test measurement with our instrument (No. 11110) showed a perfect relationship even down to 74° zenith distance (Fig. 5). Beyond that point the reflection of the direct radiation inside the glass dome that is supposed to cause the deviation from the so-called "cosine-law" (Ambach, Beschorner, Hoinkes, 1963), reaches the thermopile of the instrument (Fig. 6). This then causes a change in sensitivity. Unfortunately, it is not uniform for all azimuth angles. If the thermopile is orientated in a direction so that the reflection is falling on one of the white fields, the ratio between calculated and observed intensity increases to 1.03 at about 83° and decreases again with increasing zenith distance. However, if the reflection is falling on a black field, the ratio between calculated and observed intensity is continuously decreasing to values of 0.7 and less. Fortunately the astronomical conditions of the Colorado winter allow the thermopile to be put in a position that lets the reflection from the glass dome fall on a white field in the morning as well as in the afternoon. So the same correction could be applied to the angles above 74° regardless of the time of day.

2.4 The Meteorological Standard Instruments

The meteorological routine observations at 0900, 1200 and 1500 MST were made at the weather station of the Watershed Science Department. It was located about 100 m away from our radiometers. The readings for temperature and humidity were taken from a liquid thermometer and a hygrothermograph. For air-pressure an aneroid barograph was used. Before the project it had been compared with the mercury barometer at the CSU weather station in Fort Collins.

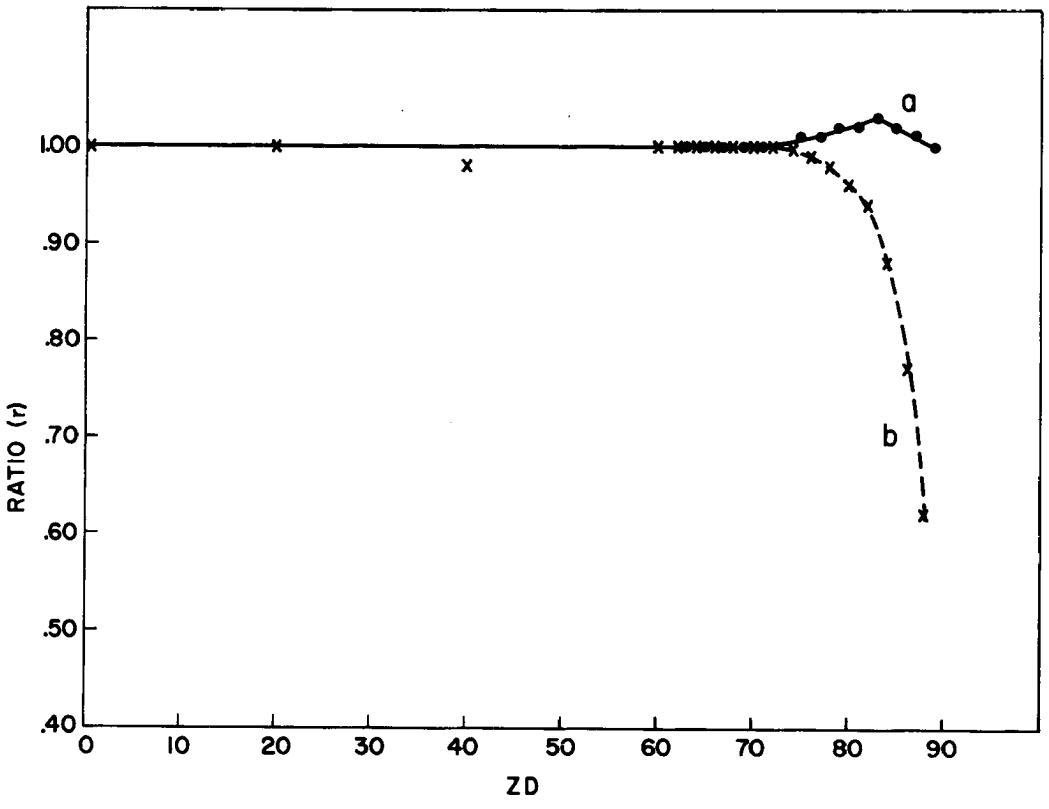

Fig. 5. The ratio (r) between the calculated intensity ($I_c = I_o/\cos ZD$) and the measured intensity (I_m). I_o = normal incidence intensity, ZD = zenith distance. (a) occurs when the black field is oriented towards the sun whereas (b) occurs when the black field is oriented away from the sun.

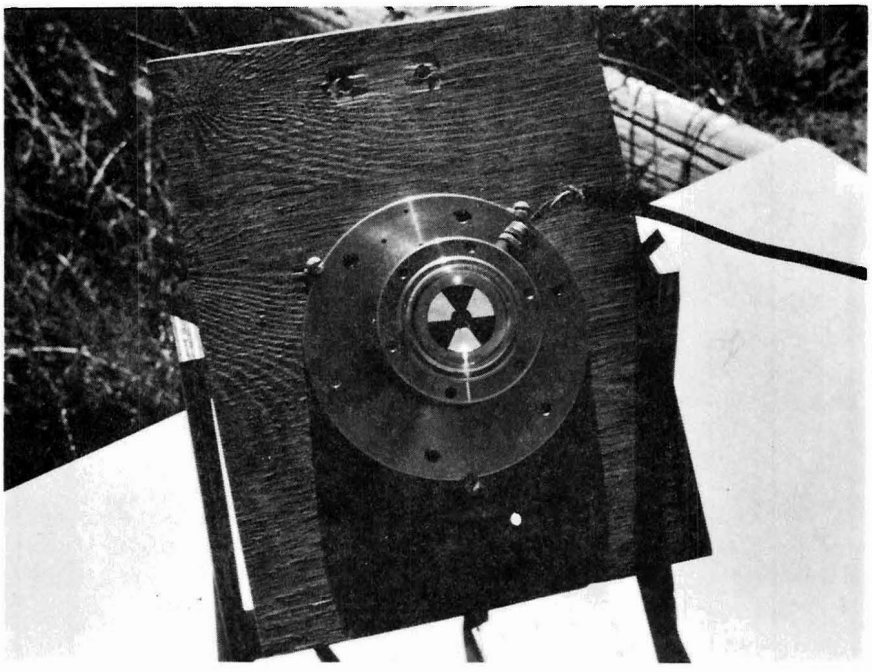

Fig. 6. Observed reflection on the thermopile of the pyranometer at a large zenith distance.

3.0 THE GEOGRAPHICAL AND ASTRONOMICAL CONDITIONS

Pingree Park is part of the upper valley of the South Fork of the Cache la Poudre River. About 2.4 km long, 0.4 km wide and orientated from southwest to northeast, it is covered by meadows with brush at the bank of the river. The instruments were installed in the northeastern part of that area at 40^{o} 34'.1 N, 105^{o} 35'.5 W and an elevation of 2740 m above sea level (U.S. Geological Survey, 1962). The horizon, as it appears at this position at 1.2 m over the ground, is given in Fig. 7.

From an azimuth angle of 55^{o} to 195^{o} (north = 360^{o}) the horizon is formed by forest covered ridges with an absolute height ranging from 2900 m in the northeast to 3700 m in the south. From 200^{o} to 235^{o} the valley is bound by a slope of snowcovered rocks. The rest of the horizon is formed by trees of Lodgepole and Ponderosa Pine, most of them standing close to the instrument site. The average elevation of the horizon is 11.1°, which would cause a reduction of 4% of the diffuse sky radiation for a completely nonreflecting surface. Measurements showed the reduction to be less.

Due to these conditions, the direct sunshine reached the instrument site a few minutes before 0800 local standard time, about 45 minutes after astronomical sunrise. Local noon occurred about 10 minutes after 12 n MST with a zenith-distance of the sun ranging from 59^{o} on the first days to 57^{o} at the end of our project. After 1600 about one hour before astronomical sunset, first shadows of the trees disturbed measurements of the albedo. Nevertheless the albedo measurements were undisturbed by the horizon up to a zenith distance of 78^{o}.

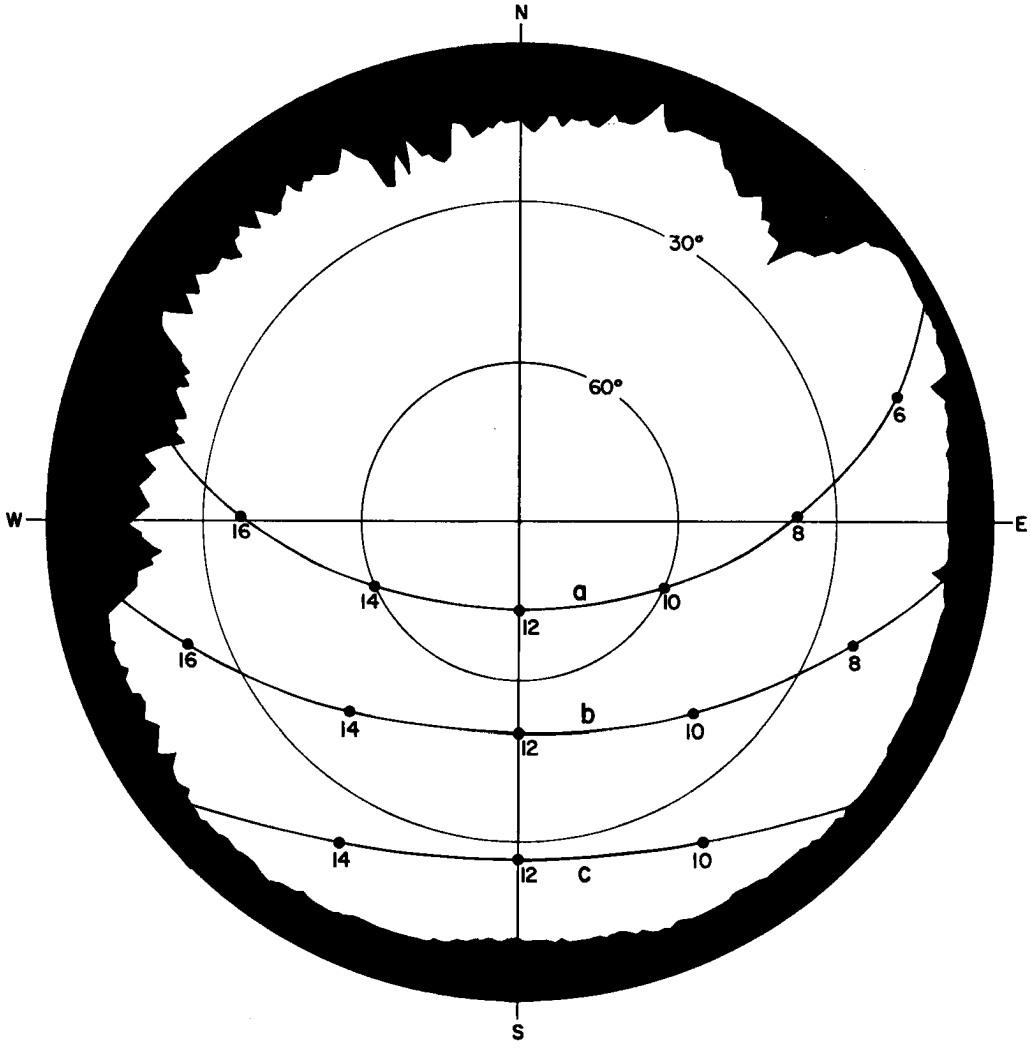

Fig. 7a. Horizon diagram of the site with solar paths for 21st June, 21st March and 23rd September, and 21st December.

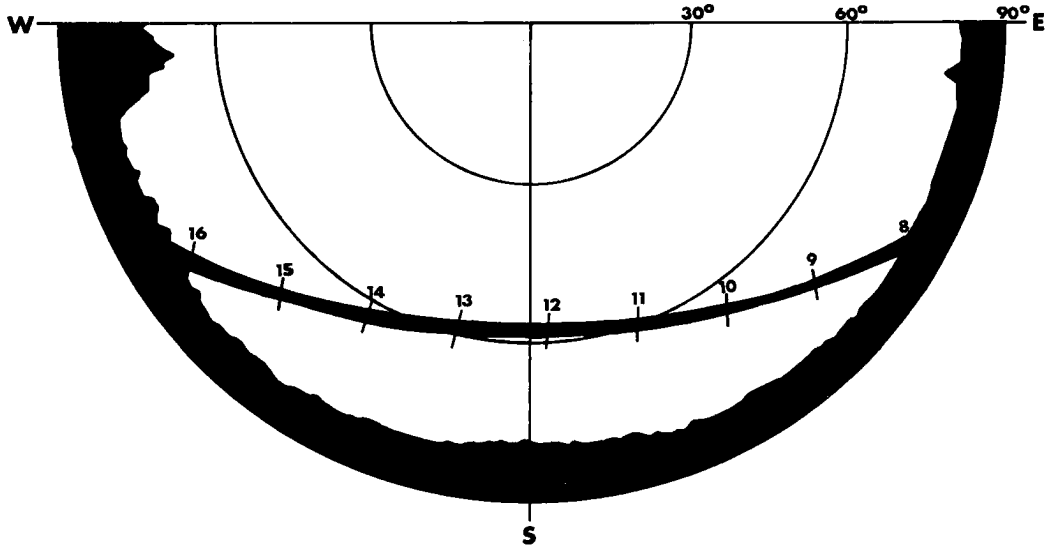

Fig. 7b. Horizon diagram with solar sun path observed during the experiment.

4.0 THE WEATHER SITUATION

4.1 The Large Scale Weather Situation

Our first weather observation on the 27th of January at 0900 MST found the sky overcast with low stratus, snowfall, a temperature of -6.7°C and an air pressure of 709 mb. The 500 mb map at that time showed a strong trough along the California Pacific coast, associated with southwesterly winds of 70 knots over Colorado. At the surface, high pressure dominated the central United States. A low center located north of Colorado drew in warm air from the south along the east slope of the Rockies. This, however, was occuring only in the lower levels leaving our mountain site under cold conditions. Thus, the temperature did not rise until noon of the 29th, after having reached a low of -16°C that morning.

During this time the upper trough as well as the surface pressure center rapidly decreased in strength while moving slowly eastward. On the 29th, surface pressures began to rise over the central and western United States, while at 500 mb the trough deepened again after it had passed over our area. This led to a divergence in the flow pattern at that level over Colorado and to clear skies for the next two days. The temperature increased during that time and stayed above the freezing level from 1000 MST on the 29th to 1500 MST on the 31st. Shortly thereafter this weather situation ended, the surface pressure already having reached its maximum in the western United States on the 30th. A new trough at 500 mb approached from the northwest. In advance of it, cold air with snow moved in on the afternoon of the 1st of February. The next day the high temperature was only -12°C with a minimum of -26°C reached shortly before sunrise.

On the 3rd of February, high pressure with a center over Idaho started to build. The 500 mb flow pattern became more zonal and warmer air moved in from the Pacific. Our last observation at 0900 MST on the 4th of February showed 5/10 Ci-Ac, opaque sun, a temperature of -1.9°C and an air pressure of 719 mb.

4.2 The Meteorological Conditions at the Measurement Site

From the large scale weather situation we received completely undisturbed conditions for the measurement of the direct solar radiation on the 30th and 31st, as well as on the morning of the 29th of January. On the afternoons of January 29th and February 2nd, and the morning of February 3rd, we found some undisturbed moments for pyrheliometric observations. During all the periods mentioned previously we could measure the turbidity of the atmosphere and calculate the reflectivity of the snow in relation to the sun position for clear sky. For the reflectivity under cloudy conditions the results from the 27th and 28th of January were used, when we had a completely overcast sky for the entire day.

On the surface of our site we could observe fresh but windpacked snow on the 27th and 28th of January. From the 29th on, it aged until new snowfall occurred in the afternoon of February 1st. On the 2nd we found fresh and completely unpacked snow until strong winds arose in the late afternoon. On the 3rd the structure of the snowfield at our site was again windpacked, while at a distance from our instruments the ground had, in spots, become entirely snow-free.

To study whether the reflectivity of snow is temperature dependent we could compare between the 29th of January, when the temperature ranged between -15°C and -10°C and the 31st, when it warmed up to +1.7°C. The remainder of the time it ranged between -10°C and 0°C during daytime. As already mentioned, the 2nd of February was the coldest day but radiation as well as snow conditions were flucuating too much for detailed observations.

5.0 Measurements

5.1 The Incoming Radiation at the Surface

To describe the radiation conditions on a clear day, we selected the results from the 31st of January. At approximately 0655 MST that day the recorder for the global radiation showed its first response. The zenith distance of the sun was then 93^{o}. From this time on the radiative intensity increased continuously until sunrise at 0800 when it rose from 0.03 ly/min to 0.18 ly/min, within six minutes. After this the continuous upward trend proceeded until it reached its maximum around local noon (between 1152 and 1230 MST) with 0.89 ly/min. At 1613 the steady path of the graph was interrupted by a nearby tree, shading off the sun for a few minutes, thus causing a sudden drop in intensity to 0.08 ly/min. Sunset occurred at 1622 with a drop in radiation from 0.20 to 0.03 ly/min. At 1725, when the sun reached a zenith distance of 93°, the recorder returned to the zero-line again

Even though the curve of the global radiation looks rather symmetric in the morning and afternoon, (see Fig. 8) a detailed comparison of the incoming radiation, before and after noon, at the same sun angle, shows that the latter values are on the average about 7% higher. To analyze this, we split up the global radiation into the direct and diffuse components. For this we used our semihourly sets of pyrheliometric measurements of solar radiation from 0930 to 1515. As a result we find the diffuse radiation fluctuating around .08 ly/min during this time interval, reaching a maximum of 0.10 ly/min at approximately 1100 hours. Therefore, the increase of global radiation is only caused by the direct solar radiation, and since the water vapor content of the atmosphere from our estimates was nearly unchanged, this asymmetry apparently resulted from the lower

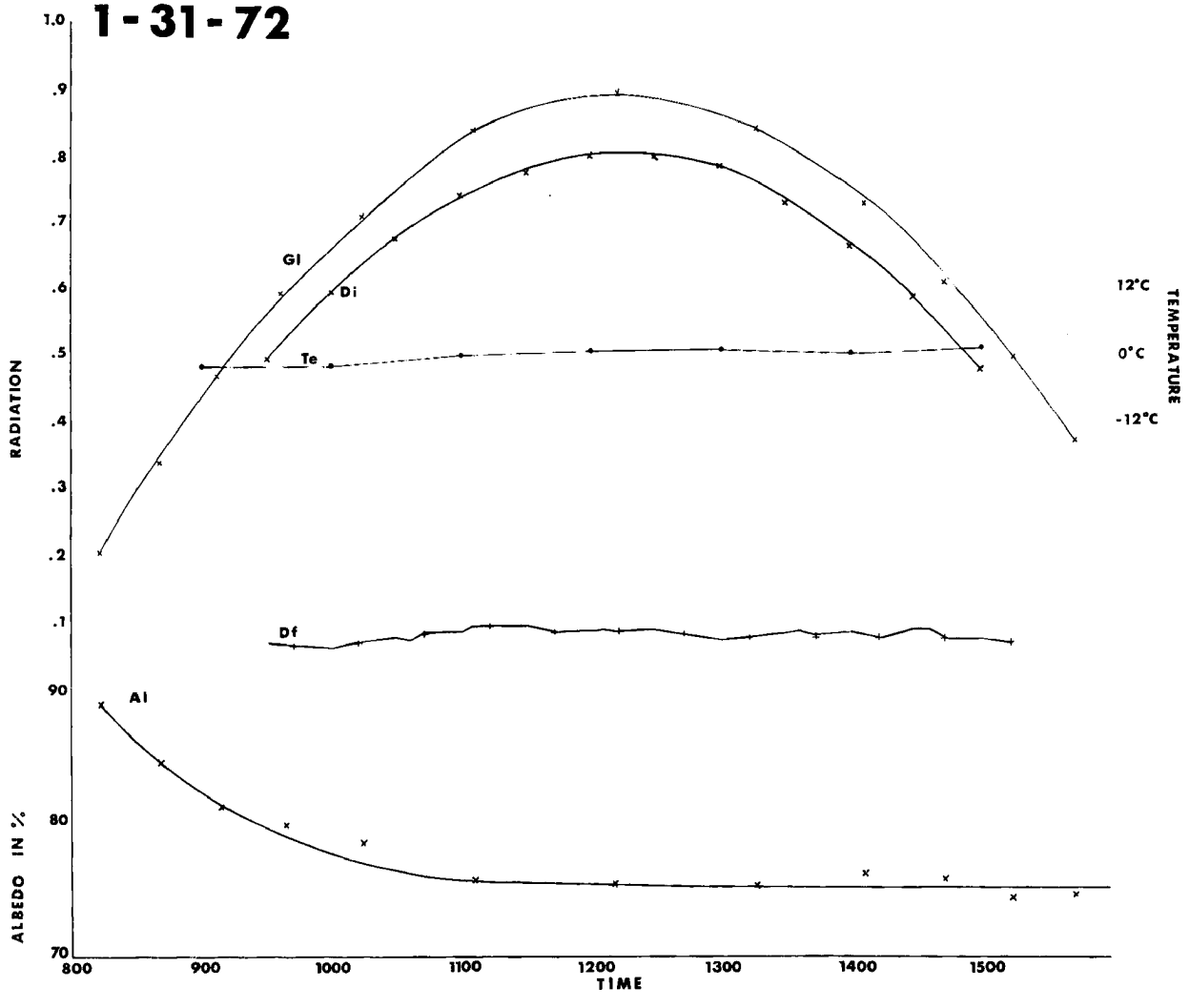

Fig. 8. Radiation, temperature (TE) and albedo (AL) on 31st of January, GL-global radiation, Di-direct radiation, Df-diffuse radiation of the sky.

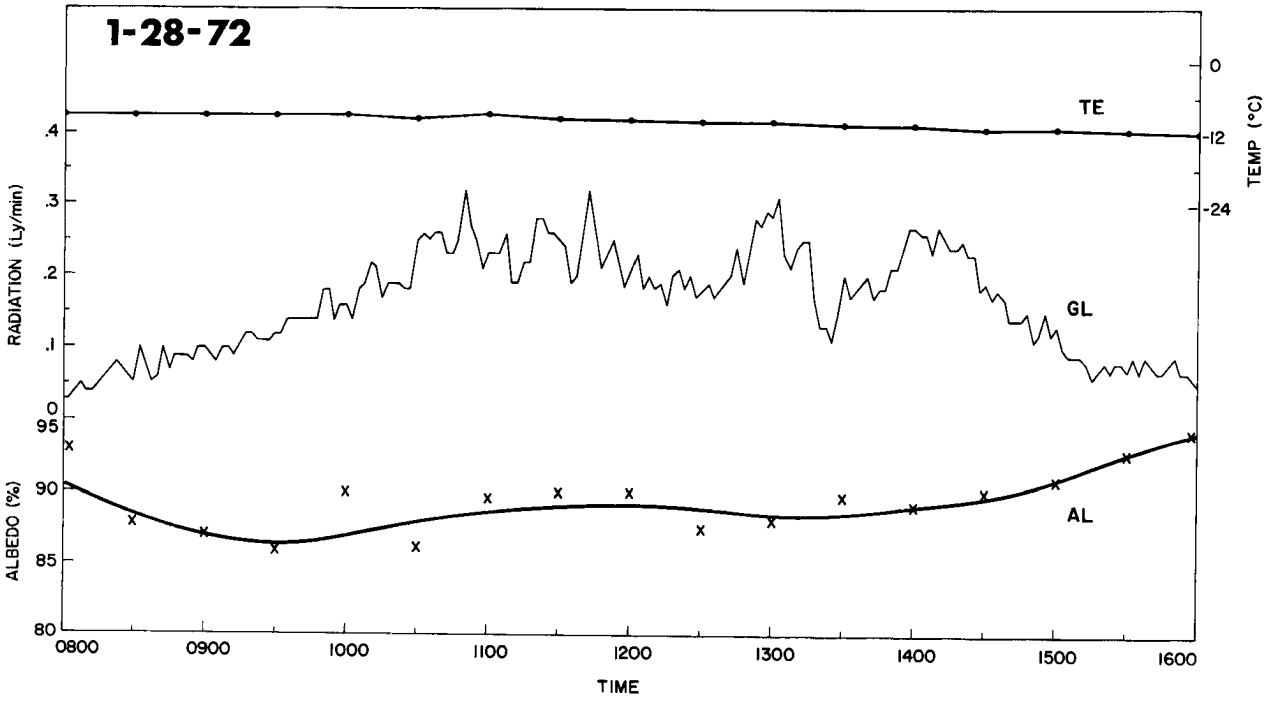

Fig. 9. Radiation, temperature (TE) and albedo (AL) on 28th of January, GL-global radiation.

turbidity at that time. Even though an opposite daily trend generally is expected, this tendency has already been observed by other authors on days with low convection in the wintertime (Foitzig and Hinzpeter, 1958). However, we believe that in our case the change is caused by a trend in the large-scale weather situation rather than by mean conditions. In this regard we observed a slight increase in turbidity (β) from the 29th to 30th of January with a maximum value for β of 0.03 at noontime. From then β dropped continuously and produced values below .005 on the afternoon of the 31st. This value is even lower than the limit that Hoelper (1939) reports for our altitude and results in a 2% higher global radiation than on the day before. For this period the weather maps show an upper air inflow from the North during three days as well as a wind velocity at the mountain crest of 10 knots compared with 40 knots on the 30th. After the 31st, turbidity measurements could only be made for a short period. While the 2nd of February still showed low β values between .01 and .02, the 3rd produced a value of approximately .035 after warm air had moved in from the West.

5.2 The Effect of Cloudiness

As important as the turbidity of the atmosphere is for the long-term heat budget, for short periods it is by far outweighed by the effect of clouds. Thus we observed a global radiation of 327 ly on the 31st of January but only 81 ly on the 28th when overcast skies occurred during the day. The duration of daylight as defined from the record of the global radiation was not much different from the cloud-free day, but the intensity was low and varying. The maximum value of 0.32 ly/min was reached several times between 1000 and 1500 hours.

5.3 The Reflectivity of the Snow Surface

For the radiation budget the incoming and reflected radiation are the two important components. While most natural surfaces absorb approximately 80% of the short-wave energy, a snowfield reflects that amount. The actual value depends on the surface conditions and the zenith angle of the sun. Thus we observed over windpacked snow on the 31st at 0813 with a solar zenith angle of 90^{o}, an albedo of 89%. From there the albedo decreased to 81% at 0923 with the zenith angle, now at 80^{o}, 75% at 1106 at 70^{o}, and final readings gave 75% at 58^{o} at local noon (1211). At that level the albedo then remained unchanged during the afternoon. This trend was observed on all days with direct solar radiation. However on cloudy days, like the 28th, the albedo stayed between 85 and 90%. Due to the low radiative intensity on that day, some variations were beyond the noise limit.

5.4 The Radiative Conditions in the Atmosphere over the Snowfield

While the results up to now describe the radiative conditions near the ground, information on the radiative transfer in the atmosphere on clear days was also obtained from our pyrheliometer measurements. In Fig. 10 we show an example of a flux diagram for January 31 at 1030. A description of the method of calculation to augment the measurement is given in Korff et al. (1974). To begin, we have to know the mean solar constant (Thekaekara, 1970) and correct it to the actual distance between the sun and earth. The water vapor content of the atmosphere was estimated to be .20 cm precipitable water calculated from the 00Z Denver Sounding. The division between the scattered and absorbed portion of incoming radiation was then made under the assumption that 10% of

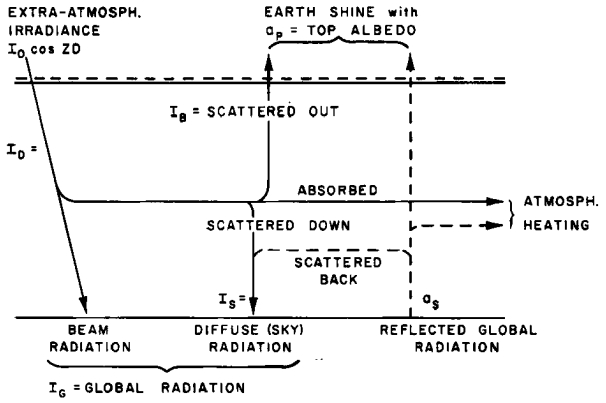

(a)

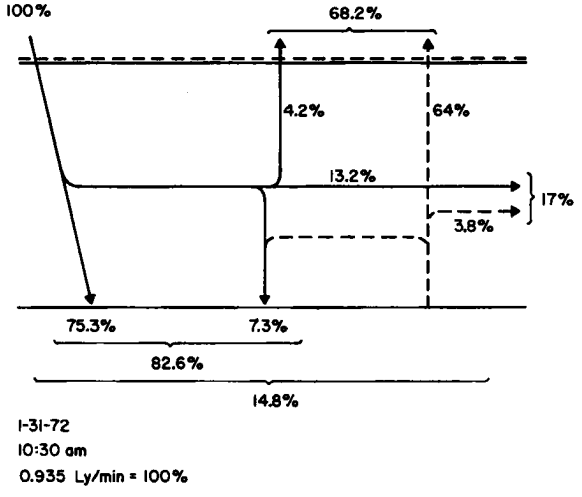

(b)

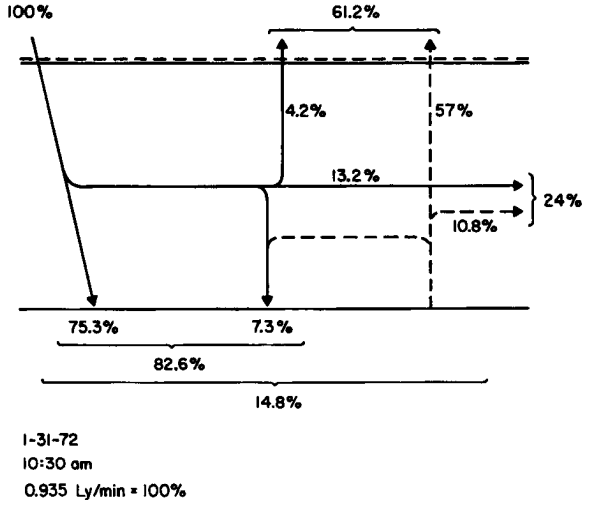

(c)

Fig. 10. Schematic illustration of the atmoshperic short-wave radiation for clear sky (31 Jan 72, 1030 MST, Pingree Park). a) notation b) pathlength of the outgoing radiation: 1 optical air mass c) pathlength of the outgoing radiation: 2 optical air masses. (after Lettau, Lettau 1969).

the extinction due to dust is absorbed and the rest scattered (Quenzel, 1971). The incoming global, direct, and diffuse radiation, as well as the absorption at the surface were measured. To separate the short-wave loss to space from the absorption of the outgoing radiation the optical pathlength has to be specified. From our results, however, this cannot be obtained. Assuming the pathlength to be 1, we derive the maximum planetary albedo and a minimum absorption value (Fig. 10b). To show how this influences the result, the same calculation is made but with a pathlength of 2 (Fig. 10c). In reality the albedo of the earth plus atmosphere system will be in between these two values with the absorption then changing by the same percentage. As a result of our minimum assumption, we obtained for January 30th a gain from short-wave radiation of 75 ly at the surface and 60 ly in the atmosphere; for January 31st, 77 ly and 62 ly respectively. Even though it is enough to provide a positive total heat budget at noontime, over the whole day the surface gain is far too low to balance the long-wave radiative loss to space in this area (Geiger, 1961).

6.0 SUMMARY

Results from an experiment to measure the short-wave radiation over a high altitude snowfield have been discussed. The albedo was determined for both clear and cloudy days, for all sun angles and shown to be higher for low sun elevations as well as somewhat asymmetric around solar noon. The results presented here are in close comparison to results by other authors and from available satellite data.

Constant care was taken to assure all equipment was calibrated and adjusted so that accurate measurements at the different short-wave components could be determined. The pyranometer and pyrheliometric data allowed us to determine the direct and diffuse radiation, as well as atmospheric turbidity so that with these parameters a future short-wave energy budget over this snowfield could be done (see Korff and Vonder Haar, 1974). These surface measurements along with satellite data available over the Antarctic and Greenland will allow a better estimate of the energy gain and loss to the earth-atmosphere system.

REFERENCES

Ambach, W., E. Beschorner, and H. Hoinkes, 1963: Über die Eichung des Strahlungsbilanzmessers nach R. Schulze (Lupolengerät). Arch. Met. Geoph. Biokl. B 13, 76-97.

Ångstrom, A. K. and A. J. Drummond, 1959: On the influence of thickness and temperature on the "cut-off" characteristics of glass filters. Quart. Journ., 85, 429-431.

Bossy, L., 1954: Etude comparative des filters actinometriques. International Radiation Conference, Rome.

Brennan, B. and W. R. Bandeen, 1970: Anisotropic reflectance characteristics of natural earth surfaces. Journ. of Applied Optics, 9, 2.

CSAGI (Comité Special de l'Anné Géophysique International) 1958: Annals of the international geophysical year 1958. Vol. 5, Part VI, Radiation Instruments and Measurements. London, Pergamon Press, 371-466.

Dirmhirn, I., 1959: Untersuchungen an Sternpyranometern. Arch. Met. Geoph. Biokl. B, 9, 124-148.

_____ and E. Trojer, 1955: Albedountersuchungen am Hintereisferner. Arch. Met. Geoph. Biokl. B, 6, 400-416.

Feubner, K., 1932: Die spektrale Durchlässigkeit der Schott' schen Filtergläser RG2 und OG1 Schmelze 20702 bzw. 12632. Meteorologische Zeitschrift 67, 242.

Foitzig, L., and H. Hinzpeter, 1958: Sonnenstrahlung und Lufttrübung. Leipzig, Akademische Verlagsgesellschaft Geest und Portig, 309 pp.

Hanson, K. J., 1960: Radiation measurement on the Antarctic snowfield, a preliminary report. J. Geoph. Res., 65, 935-946.

Hoelper, O., 1939: Atmosphärische Trübungs - und Wasserdampfbestimmung nach Filtermessungen der Sonnenstrahlung. Reichsamt für Wetterdienst, Wissenschaftliche Abhandlungen, Vol. 5, No. 10.

Hoinkes, H. C., 1961: Studies of solar radiation and albedo in the Antarctic. Arch. Met. Geoph. B, 10, 175-181.

Howard, J. N., D. E. Burch, and D. J. Williams, 1956: Infrared transmission of synthetic atmospheres. II. Absorption by carbon-dioxide. Journ. Opt. Soc. of Amer. 46, 237-241.

Inn, E. C. Y., and Y. Tanaka, 1953: Absorption coefficient of ozone in ultraviolet and visible regions. Journ. Opt. Soc. of Amer. 43, 870.

Kalitin, N. N., 1930: The measurement of the albedo of a snow cover. Mon. Wea. Rev., 58, 59-61.

Korff, H. C., 1971: Messungen zum Wärmehaushalt in den äquatorialen Anden. Annalen der Meteorologie, NF, 5, 99-102.

Lettau, H. and K. Lettau, 1969: Shortwave radiation climatonomy. Tellus, 21, 208-222.

Liljequist, G. H., 1956: Energy exchange of an Antarctic snowfield. Norwegian-British-Swedish Expedition, 1949-1952. Scientific Results, Vol. II, Part 1A, 11-109

Möller, F., 1957: Strahlung in der unteren Atmosphäre. In: S. Flügge, editor, Encyclopedia of Physics, Berlin, Springer Verlag, Vol. 48, 155-253.

Peyinghaus, W., 1972: Ein rechnerisches Verfahren zur Bestimmung der atmosphärischen Trübung aus Aktinometermessungen. Bonn, Meteorologisches Institut der Universität.

Quenzel, H., 1971: Private communication

Raschke, E., T. H. Vonder Haar, W. R. Bandeen, and M. Pasternak, 1972: The radiation balance of the earth-atmosphere system from Nimbus 3 radiation measurements (15 April 1969 - 3 February 1970). NASA Tech Note, in press.

Rusin, N. P., 1964: Meteorological and radiational regime of Antarctica. Jerusalem, Israel Program for Scientific Translations, 355 pp.

Scheibbner, F. and W. Mahringer, 1968: Die Albedo der Sonnblickgletscher und ihre zeitlichen Variationen. Arch. Met. Geoph. Biokl. B, 16, 174-194.

Shaw, G. and G. Wendler, 1972: Atmospheric turbidity measurements at McCall Glacier in Northeast Alaska. Conference on Atmospheric Radiation, Fort Collins, Colorado, 181-187.

Stanhill, G., M. Fuchs, and J. Oguntoyinbo, 1971: The accuracy of field measurements of solar reflectivity. Arch. Met. Geoph. B, 19, 113-132.

Thekaekara, M. P., 1970: Proposed standard values of the solar constant and the solar spectrum. Journ. of Environ. Sci., 13, 6-9.

U. S. Geological Survey, 1962: Pingree Park quadrangle. 7.5 minute series (topographic), N4030-W10530.

Vigroux, E., 1953: Contributions a l'étude expérimentale de l'absorption de l'ozone. Annals de Physique, 8, 709.

Vonder Haar, T. H. and E. Raschke, 1971: The reflected short-wave radiation from an elevated snowfield in summer in the Rocky Mountains. Unpublished data.

Vonder Haar, T. H. and V. Suomi, 1971: Measurements of the Earth's radiation budget from satellites during a five-year period. Part I: Extended time and space means. J. Atmos. Sci., 28, 305-314.

WMO (World Meteorological Organization),1971: Guide to meteorological instrument and observing practices. Chapter 9: Measurement of radiation and sunshine. Geneva, 4th edition.

ACKNOWLEDGMENTS

We wish to thank the College of Forestry and Natural Resources at Colorado State University for use of the Pingree Park research facility during the period of data collection, and especially Professor James Meiman and Vaughn Noonan for their many hours of logistical support.

Thanks also go to Paula Brant and Lyn Koch for their technical and secretarial assistance as well as Steve Lassman for help in computer programming.

The research was supported by the National Aeronautics and Space Administration under grant NGR-06-002-102.

APPENDIX I

THE CALIBRATION OF THE PYRANOMETER

To calibrate a pyranometer the intensity of the direct solar radiation must be known. We measured this with our normal incidence pyrheliometer and found the results that are given in column (NI) of Tables 1 and 2. The corresponding zenith distance is shown in column labeled (ZD). From (NI) and (ZD) we can find the direct radiation on a horizontal plane (Hor): NI · cos ZD = Hor. If the cosine law is valid for the pyranometer at the observed zenith distance, and for our case this is shown in Chapter 2.3, then (Hor) is the energy the instrument receives from the direct solar radiation. The output of the radiometer in mV when exposed to the undisturbed global radiation is listed under (Und). Then the direct radiation was shaded off the sensor by a disc with a diameter of 8 cm and placed at a distance of 12 cm from the instrument. This caused a reduction in output by the amount given under (Red). We had to take into account that our disc also shaded off about 6% of the sky-radiation. We subtracted this from the original reduction to get the output in mV (Dir) that is caused by the direct solar radiation (Hor) only. We then divided (Dir) by (Hor) to get the calibration factor (Cal) of our pyranometer, which showed the mV output from our instrument if it received a radiative energy of one ly/min.

Table 1

The calibration of sensor 11110

DATE & TIME	NI[ly]	ZD	Dir Hor [ly]	Pyr Und [mV]	Pyr Red [mV]	Dir [mV]	Cal [mVly^{-1}min]
2/3/72 11:51	1.519	57°23'	.8188	6.15	5.61	5.58	6.81
2/4/72 11:01	1.510	59°05'	.7758	5.78	5.28	5.25	6.77
2/4/72 11:30	1.511	57°25'	.8137	6.15	5.61	5.58	6.86

Table 2

The calibration of sensor 10958

DATE & TIME	NI[ly]	ZD	Dir Hor [ly]	Pyr Und [mV]	Pyr Red [mV]	Dir [mV]	Cal [mVly^{-1}min]
2/3/72 12:20	1.516	57°13'	.8209	6.01	5.44	5.41	6.59
2/3/72 12:40	1.518	57°35'	.8138	5.99	5.41	5.38	6.61

Unfortunately a third calibration measurement for element 10958 could not be made due to an unfavorable change of the weather on the 4th of February.

SUPPLEMENT A

As an addition to this study another experiment was carried out during the 15-18 of February 1973 at Lee Lake, a small lake in Ft. Collins, Colorado. The purpose of these measurements were to observationally determine the albedo of ice, both old and new, as well as determine the albedo versus sun angle. These results, together with the observations from Pingree Park should help determine the mean albedo over ice and snow fields over the world. Fig. 1 shows a graph at albedo versus time. It shows a maximum in albedo both near local sunrise and sunset which corresponds to other results of this type. Fig. 2 shows albedo versus solar zenith angle ζ for both clear morning and afternoon. The trend in each curve is very similar, however the amplitude of each is quite different. The morning curve shows a 6% higher albedo at a zenith distance of 82^{o} and remains higher until approximately 65^{o} zenith angle when it parallels the afternoon curve. Thus this graph points out an asymmetry in the diurnal reflectance of the ice surface and may be due to melting of a thin layer of ice at the surface.

Fig. 3 is a comparison of normalized albedo versus zenith angle for both ice and snow. The curve shows the large increase in the albedo of ice for increasing zenith angle, while the snow albedo increases at a lesser rate.

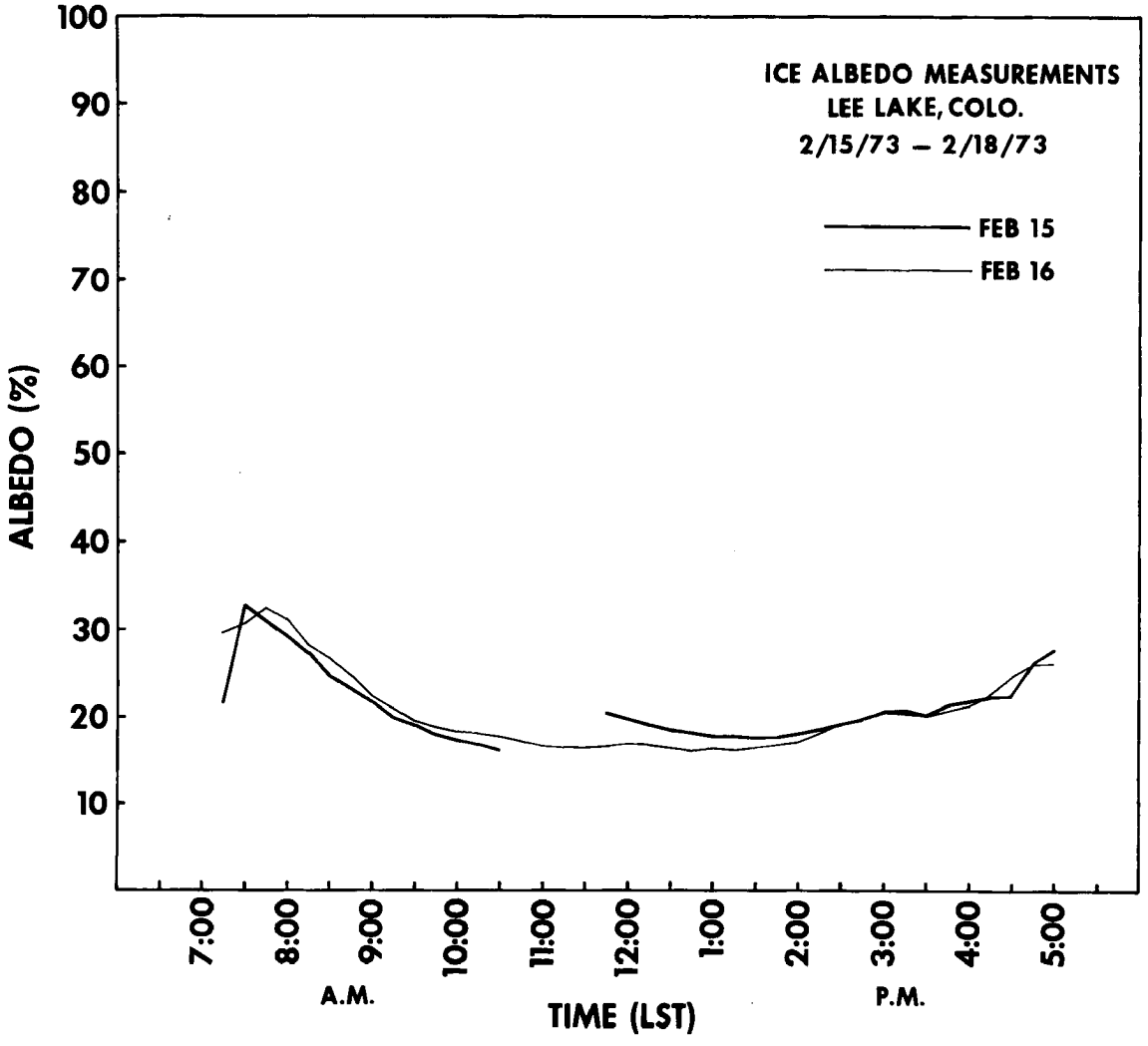
ICE ALBEDO MEASUREMENTS
LEE LAKE, COLO.
2/15/73 – 2/18/73
FEB 15
FEB 16
ALBEDO (%)
100
90
80
70
60
50
40
30
20
10
7:00
8:00
9:00
10:00
11:00
12:00
1:00
2:00
3:00
4:00
5:00
A.M.
P.M.
TIME (LST)

Figure 1

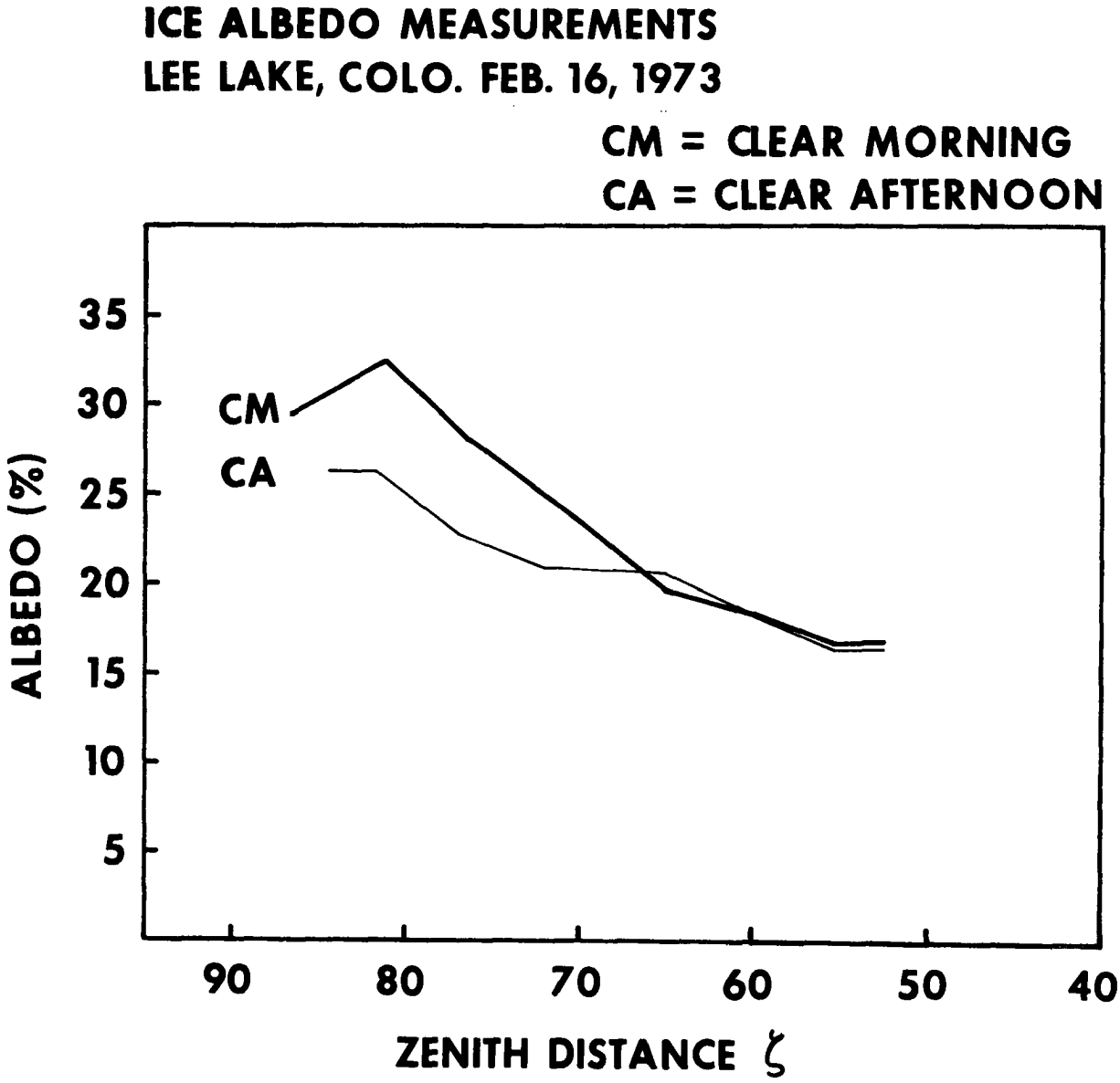
ICE ALBEDO MEASUREMENTS
LEE LAKE, COLO. FEB. 16, 1973
CM = CLEAR MORNING
CA = CLEAR AFTERNOON
ALBEDO (%)
35
30
25
20
15
10
5
CM
CA
90
80
70
60
50
40
ZENITH DISTANCE ζ

Figure 2

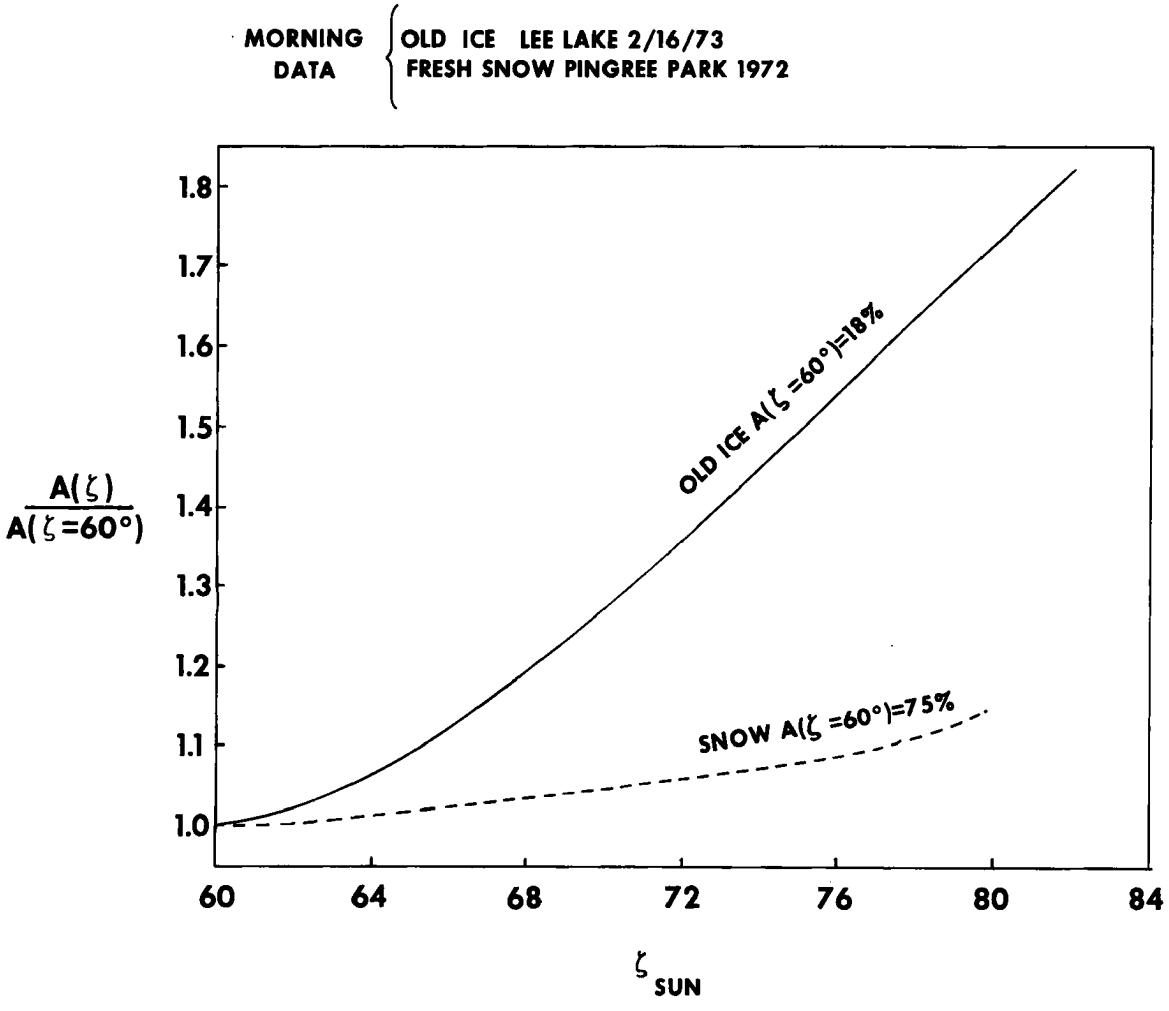
MORNING DATA
OLD ICE LEE LAKE 2/16/73
FRESH SNOW PINGREE PARK 1972
A(ζ) / A(ζ=60°)
1.8
1.7
1.6
1.5
1.4
1.3
1.2
1.1
1.0
OLD ICE A(ζ=60°)=18%
SNOW A(ζ=60°)=75%
60
64
68
72
76
80
84
ζ SUN

Figure 3

ERRATA

pg.6 $H_S = 205\ w \cdot m^{-2}$ (for $\cos \zeta_{sun} = .82$)

$M_S = 15\ w \cdot m^{-2} \cdot sr^{-1}$ for $A_{CLD} = .3$

$= 30\ w \cdot m^{-2} \cdot sr^{-1}$ for $A_{CLD} = .7$

$= 40\ w \cdot m^{-2} \cdot sr^{-1}$ for $A_{CLD} = 1.0$

$M_L = .01016\ w \cdot m^{-2} \cdot sr^{-1}$ for $A_{CLD} = .3$

$= .008160\ w \cdot m^{-2} \cdot sr^{-1}$ for $A_{CLD} = .7$

$= .003824\ w \cdot m^{-2} \cdot sr^{-1}$ for $A_{CLD} = 1.0$

$N_{CLR} = .00115\ w \cdot m^{-2} \cdot sr^{-1}$

pg. 7 $A_{CLR} = .7 - 0$

$A_{CLD} = .3 - 1.0$

$a_{CLR} = .15$

$a_{CLD} = .50$

(the N_{CLR} radiance corresponds to an effective surface temperature of $290^{o}K$)

Using the values above we evaluated equations (5) and (6) for assumed uncertainties in the measured values and for A_{CLD} ranging from .3 to 1.0.

SECTION 4 COMPLETELY REVISED - SEE FOLLOWING

4.0 RESULTS AND DISCUSSION OF UNCERTAINTY ANALYSIS

Results of the uncertainty analysis for cloud amount (A_{CLD}) show that M_S and H_S contribute most to the uncertainty in A_{CLD}. We can assume H_S, the incoming solar radiation, has little uncertainty, at most 5%; M_S has a much higher uncertainty - in the 10-20% range. The bi-directional reflectances (ρ) of the clear and cloudy regions are also at the 10-20% uncertainty level. Thus, using both an optimistic and a conservative approach we obtain:

		Conservative	Optimistic
		5% H_S	1% H_S
		20% M_S, ρ_{CLR}, ρ_{CLD}	10% M_S, ρ_{CLR}, ρ_{CLD}
A_{CLD}	A_{CLR}	ΔA_{CLD}	ΔA_{CLD}
.3	.7	.23	.1
.7	.3	.45	.3
1.0	0	.60	.28

Results of the uncertainty analysis for determining cloud top temperature (N_{CLD}) showed that A_{CLD} contributed most to the uncertainty. From previous results by Conlan (1973), M_L has an accuracy to within 1-2%. A_{CLD} has an accuracy of 30-75% as shown above. N_{CLR} has an uncertainty close to that of M_L with variations in surface topography (within the field of view) increasing it to the 5% level. Thus using conservative estimates of 5% error for M_L and N_{CLR} and the error as shown above for A_{CLD} we obtain:

		Conservative		Optimistic	
		5% M_L, N_{CLR}		1% M_L, N_{CLR}	
		A_{CLD} Above		A_{CLD} Above	
A_{CLD}	A_{CLR}	ΔT_{eff}	ΔZ	ΔT_{eff}	ΔZ
.3	.7	39^oC	5.2 km	16^oC	3 km
.7	.3	29^oC	4.2 km	12^oC	2 km
1.0	0	34^oC	4.8 km	14^oC	3 km

The results show that determining cloud amount and cloud height, within the field of view of the sensor (for a single spot) is marginal. However, if ten spots are averaged, the errors are reduced by an order of magnitude[1]. Thus we have proceeded with a test of this method by averaging an array of scan spots and comparing results to ground observations. As a further test of this uncertainty analysis, Appendix 1 contains a comparison of simultaneous satellite radiance measurements and ground based measurements to test the satellite's accuracy and stability.

Conlan, E. F., 1973: Operational products from ITOS Scanning Radiometer Data. NOAA Tech. Memo. NESS 52.

[1]The method used here was to sum the absolute values of each error term. To arrive at a gross estimation of error for an averaged array of data, divide the errors in A_{CLD} and N_{CLD} by N , the number of points.